Regular article

# Study of infrared photodetectors with wavelength extension mechanism

D. Chauhan[a], A.G.U. Perera[a],[*], L.H. Li[b], L. Chen[b], E.H. Linfield[b]

[a] *Center for Nano-Optics (CeNO), Department of Physics and Astronomy, Georgia State University, Atlanta, GA 30303, USA*
[b] *School of Electronic and Electrical Engineering, University of Leeds, Leeds LS2 9JT, United Kingdom*

ARTICLE INFO

ABSTRACT

The III-V semiconductor heterostructure-based photodetectors have been studied extensively for infrared detection, from near-infrared (NIR) to far-infrared (FIR) region. Due to the mature material system, GaAs/Al$_x$Ga$_{1-x}$As heterostructures are attractive options for development of infrared detectors. The conventional rule of photodetection, $\lambda_t = hc/\Delta$, determines the wavelength threshold ($\lambda_t$) of spectral photoresponse, where $\Delta$ is the minimum energy gap of the material, or the interfacial energy gap of the heterostructure. In recent studies on the p-GaAs/Al$_x$Ga$_{1-x}$As heterostructure-based infrared photodetectors, spectral threshold limit due to $\Delta$ has been overcome owing to a detection mechanism arising from the hot-carrier effect driven extended wavelength photoresponse mechanism. It has been experimentally observed that a detector with a conventional spectral threshold of ~3.1 μm shows an extended wavelength threshold of up to ~68 μm. An important advantage of the wavelength extension mechanism is the lower dark current, which is determined by the designed $\Delta$. Dark current fittings obtained from a 3D carrier drift model closely agree with experimentally measured dark current. A barrier energy offset ($\delta E_v$) between Al$_x$Ga$_{1-x}$As barriers is found to be necessary for the spectral extension mechanism.

## 1. Introduction

In infrared (IR) photodetectors, the spectral rule $\lambda_t = hc/\Delta$ plays a fundamental role [1] that determines the spectral threshold of photoresponse, where $\Delta$ is the energy gap of the material or heterostructure corresponding to a minimum energy of the photons that can be absorbed to produce a photocurrent, and $\lambda_t$ is the wavelength threshold. In p-type doped III-V semiconductors such as p-GaAs, IR photo-absorption results in hole transitions from the heavy-hole/ light-hole bands to the spin-orbit split-off band, and from the heavy-hole to the light-hole band [2]. Furthermore, free-carrier absorption increases with the wavelength [3] as $\lambda^2$. Using the p-GaAs/Al$_x$Ga$_{1-x}$As heterostructures for the internal photo-emission, $\lambda_t$ can be tuned by changing the Al mole fraction $x$ in the Al$_x$Ga$_{1-x}$As barrier region to design the detectors covering mid-IR to far-IR ranges [4,5]. Unlike these conventional approaches, an alternative mechanism was discovered that demonstrated an extended wavelength photoresponse in the spectral range to very-long-wavelength IR (VLWIR) range, far beyond the limit of $\Delta$ in corresponding to mid–IR range [6–8]. More specifically, a photoresponse was observed up to a $\lambda_t$ ~55 μm in a p-GaAs/Al$_x$Ga$_{1-x}$As heterostructure-based IR detector with interfacial energy gap of $\Delta$ ~ 0.40 eV (~3.1 μm). The extended wavelength photoresponse was attributed to the hot-carrier redistribution in the p-GaAs absorber/emitters layer

leading to a quasi-Fermi level at a higher energy level compared to the equilibrium Fermi level [6]. As a result, the effective energy gap $\Delta$ becomes smaller, enabling the detection of extended wavelength IR radiation. Typical detector architecture used in these studies include p-type doped GaAs absorber/emitter and undoped Al$_x$Ga$_{1-x}$As barriers, sandwiched between highly doped p-GaAs top and bottom contact layers that also serve as collector and injector respectively. A barrier energy offset ($\delta E_v$), that is, a difference between the injector and collector barrier energy, was found to be necessary condition for the extended wavelength photoresponse mechanism, evident from the fact that extended wavelength photoresponse was not observed on a reference detector with no barrier offset. Furthermore, the extended wavelength photoresponse was observed in detectors with graded and constant shapes of the injector barrier [7]. Whilst the extended wavelength threshold can be observed up to VLWIR spectral range, the measured dark current of the detector agrees closely with modelled dark current with $\Delta$ ~ 0.40 eV (~3.1 μm), which is the interfacial energy gap of the detector under equilibrium condition [8]. In this article, we present results of a comparative study of five p-GaAs/Al$_x$Ga$_{1-x}$As heterostructures-based IR photodetectors. The results highlight that the barrier offset is a critical requirement for the extended wavelength photoresponse, and the graded barrier shows higher extended wavelength photoresponse. In addition, the barrier energy offset increased

* Corresponding author.
  *E-mail address:* uperera@gsu.edu (A.G.U. Perera).

**Table 1**
Summary of sample parameters: Emitters in all samples have the doping level of $1 \times 10^{19}\,\mathrm{cm^{-3}}$, except for $3 \times 10^{18}\,\mathrm{cm^{-3}}$ in SP1.

| Sample | $\Delta$ (eV) (designed) | Energy offset ($\delta E$) (eV) | Al mole fraction $x_1, x_2, x_3 = x_4$ | $w_e$ (nm) | $w_1$ (nm) | $w_2$ (nm) | Number of Periods (N) |
|---|---|---|---|---|---|---|---|
| SP1001 | 0.40 | 0.10 | 0.75, 0.75, 0.57 | 80 | 80 | 400 | 1 |
| SP1007 | 0.40 | 0.10 | 0.45, 0.75, 0.57 | 80 | 80 | 400 | 1 |
| 15SP3 | 0.40 | 0.19 | 0.45, 0.75, 0.39 | 80 | 80 | 400 | 1 |
| LH1002 | 0.30 | None | 0.57, 0.57, 0.57 | 20 | 60 | 60 | 1 |
| SP1 | 0.157 | None | 0.28, 0.28, 0.28 | 20 | 60 | 60 | 30 |

from 0.10 eV to 0.19 eV enables increased photoresponse and optimized operating condition over a wide applied bias range. Furthermore, a comparison of dark current with a conventional detector shows a significant dark current advantage due to the extended wavelength mechanism.

## 2. Experiments

Five samples - SP1001, SP1007, 15SP3, LH1002, and SP1 were grown by molecular beam epitaxy on semi-insulating GaAs substrate. The parameters of these heterostructures are summarized in Table 1. In the samples SP1001, SP1007, and 15SP3, the p-GaAs emitters are 80 nm, and $Al_xGa_{1-x}As$ barriers are 80 nm and 400 nm below and above the emitter respectively. The 400 nm $Al_xGa_{1-x}As$ barrier is constant in all three samples. The 80 nm $Al_xGa_{1-x}As$ barrier is constant in SP1001, but in SP1007, and 15SP3, barrier energy profile is graded by linearly varying the Al mole fraction from $x_1 = 0.45$ at lower edge of the barrier to $x_2 = 0.75$ at the upper edge. The constant barrier in SP1001 and SP1007 have $x_3 = x_4 = 0.57$, but 15SP3 has $x_3 = x_4 = 0.39$. Thus, SP1001 and SP1007 have the barrier offset $\delta E_v = 0.10$ eV and 0.19 eV respectively. Samples LH1002 and SP1 are used as reference detectors without the barrier offset. The constant $Al_xGa_{1-x}As$ barriers in all the samples have $x_1 = x_2 = x_3 = x_4 = 0.57$ and 0.28 in LH1002 and SP1 respectively. The interfacial energy gap in SP1001, SP1007, and 15SP3 is $\Delta \sim 0.40$ eV, whereas $\Delta \sim 0.30$ eV and 0.157 eV in LH1002 and SP1 respectively. The emitter doping level in all samples are $1 \times 10^{19}\,\mathrm{cm^{-3}}$, except for $3 \times 10^{18}\,\mathrm{cm^{-3}}$ in SP1. The equilibrium valence band alignment of the heterostructures are depicted in Fig. 1(a)–(c). Detector mesas of $400 \times 400\,\mu m^2$ were fabricated by conventional photolithography and wet etching. Ti/Au metallic ring contacts were evaporated on the top and bottom contact layers. An optical window of $260 \times 260\,\mu m^2$ was opened on the top contact layer for normal incident optical illumination.

Dark current (I-V-T) characteristics were measured using Keithley 2635B source meter. A positive bias is a positive voltage connected to the top contact, with the bottom contact grounded. Similarly, a negative bias is the positive voltage connected to the bottom contact, with the top contact grounded. Spectral photoresponse was measured using a Perkin-Elmer system 2000 FTIR set up. A bolometer with known sensitivity was used to measure the background intensity of the blackbody source to calibrate the responsivity of detectors

## 3. Results and discussion

An extended wavelength photoresponse was observed in the samples SP1001, SP1007, 15SP3 measured at 5.3 K, as shown in Fig. 2. Note that the samples SP1001 and SP1007 have the same barrier offset ($\delta E_v = 0.10$ eV), but SP1007 has graded injector barrier as opposed to a constant injection barrier in SP1001. Also, the spectral photoresponse used for the comparison are chosen from the optimal signal of each sample. SP1007 had an extended wavelength photoresponse in a small range of applied biases, less than $-0.2$ V in magnitude, as reported previously in Ref [6]. SP1001 showed the photoresponse on the extended wavelength regime in the applied biases of $-0.6$ V or less in magnitude. The comparison shows that a higher photoresponse was observed in SP1007 than in SP1001. Similarly, wavelength threshold is slightly longer in SP1007 ($\sim 56\,\mu m$) compared to SP1001 ($\sim 50\,\mu m$). The wavelength threshold of the photoresponse was determined by using the temperature dependent internal photoemission spectroscopy (TDIPS) method [9]. In this method, the value of the energy ($\Delta$) corresponding to the spectral threshold of the photoresponse is determined by obtaining a fitting for quantum yield, $Y(h\nu) \sim (h\nu - \Delta)^2$, in the near-threshold region. The wavelength threshold for 15SP3 was found to be $\sim 59\,\mu m$. The results from these three samples indicate that the barrier energy offset gives rise to an extended wavelength mechanism, which enabled the VLWIR photoresponse. However, the three samples show
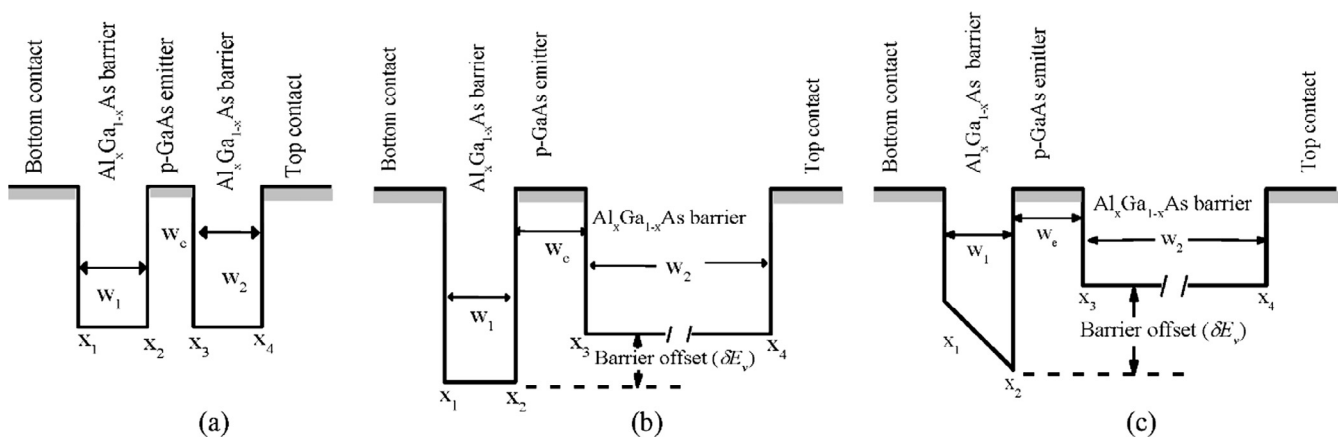


**Fig. 1.** Schematic diagrams of the valence band alignment of the detectors under equilibrium: (a) detectors without barrier offset: LH1002 has one period and SP1 and 30 periods of 20 nm p-GaAs and 60 nm $Al_xGa_{1-x}As$ barriers. (b) SP1001 consists of an emitter (80 nm), an 80 nm $Al_{0.75}Ga_{0.25}As$ barrier at the bottom, and a 400 nm $Al_{0.57}Ga_{0.43}As$ barrier at the top, with an energy offset ($\delta E_v$) of $\sim 0.10$ eV between the barriers. (c) In SP1007 and 15SP3 have $Al_xGa_{1-x}As$ barrier (80 nm) at the bottom is graded by tuning the Al mole fraction from from $x_1 = 0.45$ at lower edge of the barrier to $x_2 = 0.75$ at the upper edge. The constant barrier in SP1001 and SP1007 have $x_3 = x_4 = 0.57$, but 15SP3 has $x_3 = x_4 = 0.39$. SP1001 and SP1007 have the barrier offset $\delta E_v = 0.10$ eV and 0.19 eV respectively. The emitters are thick enough so that there will a bulk-like distribution of energy states.
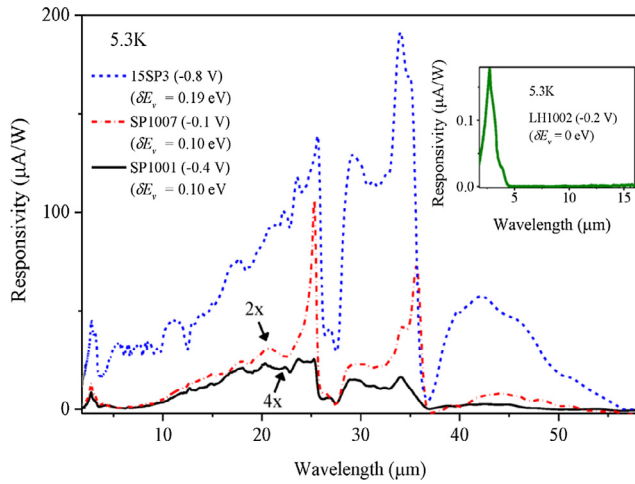
Fig. 2. Spectral photoresponse of samples SP1001, SP1007, and 15SP3 measured at 5.3 K shows the wavelength threshold of 50, 56, and 59 μm respectively whilst the interfacial energy gap is Δ ~ 0.40 eV (~3.1 μm) for all three samples. Note that the responsivity of SP1001 and SP1007 are multiplied 4 and 2 times respectively for better visualization. Inset shows the photoresponse of the reference detector LH1002 with Δ ~ 0.30 eV (~4.1 μm), without an extended wavelength photoresponse. The comparison is based on the optimal signal of each sample. SP1007 had an extended wavelength photoresponse in a small range of applied biases less than -0.2 V, as reported previously in Ref [6]. Similarly, SP1001 showed the extended wavelength photoresponse in the range of applied biases of −0.6 V or less.

only a small variation in the wavelength threshold. On the other hand, the spectral responsivity was found to improve significantly due to the graded barrier in SP1007 compared to the constant barrier structure in SP1001. Furthermore, with the barrier offset increased to $\delta E_v = 0.19$ eV in 15SP3 compared to $\delta E_v = 0.10$ eV in SP1007, the spectral responsivity was found to improve by more than a two-fold factor. Note that the improvements in the spectral responsivity is more pronounced in the VLWIR region. In contrast, the reference detector LH1002 did not show the extended wavelength photoresponse. The wavelength threshold of ~4.1 μm closely agrees with the interfacial energy gap of Δ ~ 0.30 eV, as shown in inset of Fig. 2.

Although the extended wavelength photoresponse in SP1007 was observed in a narrow range of negative bias, sample 15SP3 (with a higher barrier offset) showed the extended wavelength photoresponse in a wider applied bias range, including positive biases. As shown in Fig. 3, a strong photoresponse was observed under positive bias, with
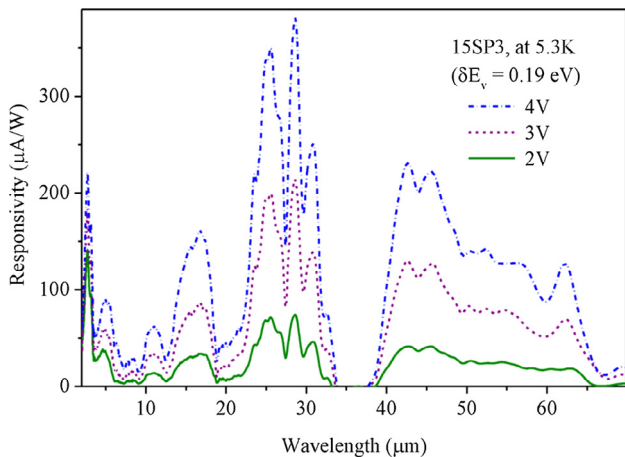


Fig. 3. Spectral photoresponse of 15SP3 sample under positive applied biases. Extended wavelength threshold was found to be ~68 μm, at 4 V, as determined from TDIPS method.
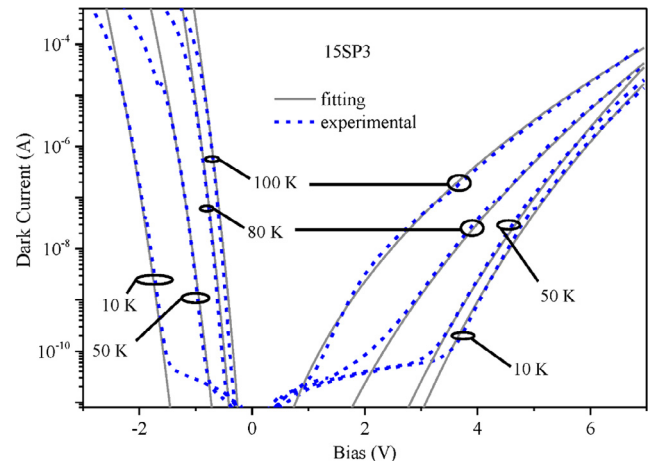


Fig. 4. The fitted dark current for sample 15SP3 closely agrees with the measured dark current. A 3D carrier drift model was applied to fit the dark current, with Δ ~ 0.40 eV.

the extended wavelength threshold ~68 μm at 4 V, at 5.3 K. These results suggest that the barrier offset is not only the necessary condition for the extended wavelength photoresponse mechanism, but also the higher value of the offset is more optimized parameter for the operation of the extended wavelength photodetectors.

In addition to the photoresponse analysis, we applied fittings to measured dark currents from 10 to 100 K for 15SP3, as shown in Fig. 4. To obtain the fittings, a 3D carrier drift model [8,10] as shown in Eq. (1) was used.

$$I_{dark} = Ae \frac{\mu F}{\left[1 + \left(\frac{\mu F}{v_{sat}}\right)^2\right]^{1/2}} 2\left(\frac{m^* k_B T}{2\pi \hbar^2}\right)^{3/2} \times \exp\left(-\frac{\Delta - \alpha F - E_f}{k_B T}\right)$$

(1)

Here, $A$ is the electrically active area of the detector, $e$ is the electronic charge, $\mu(F)$ is the hole drift velocity as function of applied field, $v_{sat}$ is the saturation velocity, $m^*$ is the effective mass, $k_B$ is Boltzmann's constant, $T$ is temperature, $\hbar$ is the reduced Planck constant, $\alpha$ is a fitting parameter related to barrier lowering due to the applied field, and $E_f$ is the Fermi level. Details of the 3D carrier drift model used for dark current fitting are reported in Ref [8,10]. As seen in Fig. 4, the fitted dark current closely agrees with the measured dark current for 15SP3 with Δ ~ 0.40 eV. We note that the experimentally measured dark current deviates only for small values of the applied biases, and mostly for positive bias conditions. One of the possible reasons for this behavior may be attributed to the non-uniform distribution of the applied bias due to presence of multiple resistive elements [4,11], that is, energy barriers with different barrier heights. At low biases, mostly the dc voltage is dropped across the graded barrier due to higher barrier energy, making the effective electric field across it much higher than the value under uniform distribution. This means the measured dark current would be higher than predicted by the model. The dc resistance of the high resistive element decreases as the bias increases, causing redistribution of dc voltage to constant barrier (with smaller barrier height) too, hence the measured dark current approaches the values predicted by the model. Overall, the results confirm that the dark current in the extended wavelength IR photodetectors is determined by the equilibrium interfacial energy, which is much larger than the actual energy corresponding to the extended wavelength threshold (~68 μm). In other words, there is no compromise in terms of dark current due to the wavelength extension mechanism.

The next comparison of photoresponse and dark current in the conventional IR photodetector (SP1) and the extended wavelength IR photodetector (SP1007) is shown in Fig. 5(a) and (b) for measurements carried out at 50 K. In SP1, the wavelength threshold (~8.2 μm) closely
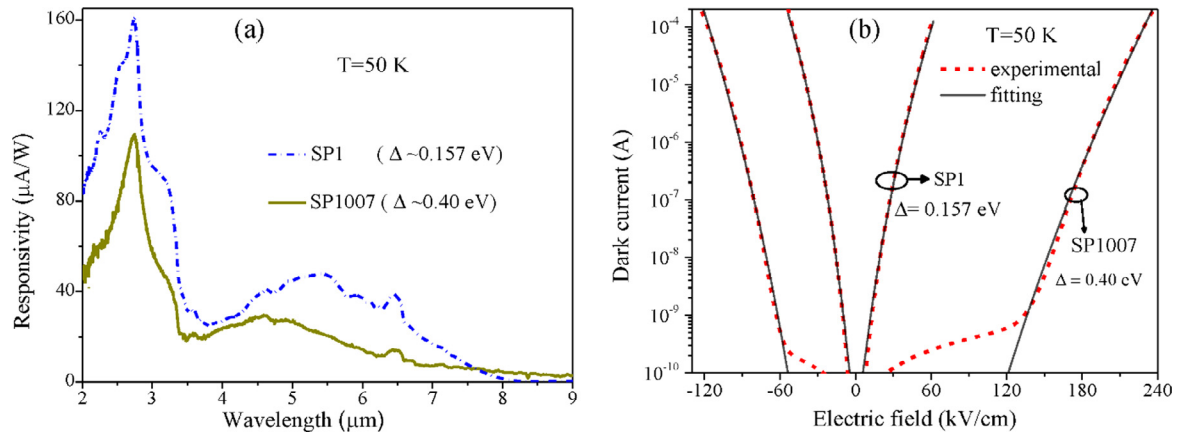
**Fig. 5.** A comparison of conventional IR photodetector SP1 with extended wavelength IR photodetector AT 50 K. (a) SP1 with $\Delta \sim 0.157$ eV ($\sim 8.2$ μm) shows no extended wavelength photoresponse, but SP1007 with $\Delta \sim 0.40$ eV ($\sim 3.1$ μm) shows an extended wavelength photoresponse up to $\sim 8.9$ μm. (b) The fitted dark currents with $\Delta \sim 0.40$ eV and 0.157 eV for SP1007 and SP1, respectively, closely agree with the measured dark currents. The results demonstrate that the extended wavelength photoresponse mechanism offer significant dark current advantage over the conventional IR photodetector when operating in the similar spectral range.

agrees with $\Delta \sim 0.157$ eV. However, SP1007 shows an extended wavelength threshold of 8.9 μm. Given that the observed photoresponse in these two samples are similar to each other at 50 K, it is insightful to compare the dark current of these samples. The fitted dark current agreed closely with the measure dark current in both SP1 ($\Delta \sim 0.157$ eV) and SP1007 ($\Delta \sim 0.40$ eV) as seen in Fig. 5(b). Note that the dark current in extended wavelength IR photodetector SP1007 is significantly lower than the conventional photodetector SP1. These results also demonstrate the dark current advantage of extended wavelength photoresponse mechanism.

### 4. Conclusion

The study of p-GaAs/Al$_x$Ga$_{1-x}$As heterostructures-based extended wavelength IR photodetectors with reference to conventional IR photodetectors demonstrate that the heterostructures with a barrier energy offset ($\delta E_v$) is a critical requirement for the wavelength extension photoresponse mechanism. This mechanism enabled a VLWIR detection, with wavelength threshold of $\sim 68$ μm at 5.3 K even though the heterostructures had an equilibrium interfacial energy gap of $\Delta \sim 0.40$ eV ($\sim 3.1$ μm). The dark current fittings obtained using a 3D carrier drift model, with $\Delta \sim 0.40$ eV, agreed closely to the measured dark currents, indicating no compromise in the dark current levels due to the wavelength extension mechanism.

### Conflict of interest

The authors declared that there is no conflict of interest

### Acknowledgements

### References

[1] S.M. Sze, K.K. Ng, Physics of semiconductor devices, 3rd ed., Hoboken, N.J., Wiley-Interscience, 2007.

[2] Y.F. Lao, P.K.D.D.P. Pitigala, A.G.U. Perera, H.C. Liu, M. Buchanan, Z.R. Wasilewski, K.K. Choi, P. Wijewarnasuriya, Light-hole and heavy-hole transitions for high-temperature long-wavelength infrared detection, Appl. Phys. Lett. 97 (2010) 091104–91113.

[3] A.L. Korotkov, A.G.U. Perera, W.Z. Shen, J. Herfort, K.H. Ploog, W.J. Schaff, H.C. Liu, Free-carrier absorption in Be- and C-doped GaAs epilayers and far infrared detector applications, J. Appl. Phys. 89 (2001) 3295–3300.

[4] D. Chauhan, A.G.U. Perera, L.H. Li, L. Chen, E.H. Linfield, Effect of a current blocking barrier on a 2–6 μm p-GaAs/AlGaAs heterojunction infrared detector, Appl. Phys. Lett. 108 (2016) 201105.

[5] D.G. Esaev, M.B.M. Rinzan, S.G. Matsik, A.G.U. Perera, Design and optimization of GaAs/AlGaAs heterojunction infrared detectors, J. Appl. Phys. 96 (2004) 4588–4597.

[6] Y.-F. Lao, A.G.U. Perera, L.H. Li, S.P. Khanna, E.H. Linfield, H.C. Liu, Tunable hot-carrier photodetection beyond the bandgap spectral limit, Nat Photon 8 (2014) 412–418.

[7] D. Chauhan, A.G.U. Perera, L. Li, L. Chen, S.P. Khanna, E.H. Linfield, Extended wavelength infrared photodetectors, Opt. Eng. 56 (2017) (091605 091605).

[8] D. Chauhan, A.G.U. Perera, L.H. Li, L. Chen, E.H. Linfield, Dark current and photoresponse characteristics of extended wavelength infrared photodetectors, J. of Appl. Phys. 122 (2017) 024501.

[9] Y.-F. Lao, A.G.U. Perera, Temperature-dependent internal photoemission probe for band parameters, Phys. Rev. B 86 (2012) 195315.

[10] E.R. Weber, R.K. Willardson, H.C. Liu, F. Capasso, Intersubband transitions in quantum wells: physics and device applications, Elsevier Science, 1999.

[11] H.C. Liu, J. Li, J.R. Thompson, Z.R. Wasilewski, M. Buchanan, J.G. Simmons, Multicolor voltage tunable quantum-well infrared photodetector, IEEE Trans. on Electron Devices 40 (11) (1993) 2142.